International Journal of Innovative Computing, Information and Control
Volume **8**, Number **7(A)**, July **2012**

ICIC International ©2012 ISSN 1349-4198
pp. 4851–4868

FRACTIONAL ORDER INTEGRAL SLIDING-MODE FLUX OBSERVER FOR DIRECT FIELD-ORIENTED INDUCTION MACHINES

Yeong-Hwa Chang[1], Chun-I Wu[1], Hung-Wei Lin[2], Hung-Chih Chen[1] and Chia-Wen Chang[1]

[1]Department of Electrical Engineering
Chang Gung University
No. 259, Wen-Hwa 1st Road, Kwei-shan, Tao-Yuan 333, Taiwan
yhchang@mail.cgu.edu.tw

[2]Department of Electrical Engineering
Lee-Ming Institute of Technology
2-2, Lijuan Road, Liming, Taishan, Taipei 24305, Taiwan
kinglin@yahoo.com

Received March 2011; revised September 2011

Abstract. *In field-oriented induction machines, an accurate flux estimation is crucial for high-performance speed control. However, the flux estimation is sensitive to parameter variations such that the control performance will be deteriorated. This paper presents a novel flux observer, fractional order integral sliding-mode (FOISM) flux observer, to estimate the d- and q-axis fluxes in the stationary reference frame. The closed-loop stability is guaranteed by employing the Lyapunov stability theory. Essential properties of fractional operators are also discussed for realizing fractional order integrations and differentiations properly. In addition to numerical analyses and simulations, a DSP/FPGA based experimental platform is set up to evaluate the feasibility of the proposed control framework. Simulation results indicate that the use of fractional-order schemes leads to better results than the counterparts of integer-order approaches. Also, experimental results demonstrate that the desired speed and flux tracking of an induction machine can be performed by utilizing the FOISM flux observer.*

Keywords: Fractional order, Integral sliding-mode, Flux observer, Field-oriented control, Induction motor, DSP/FPGA

1. **Introduction.** Because of highly nonlinear characteristics, coupling and time-varying dynamics, the control of induction motors is much more difficult than the counterpart of DC motors. In this context, the field-oriented control scheme, also called the vector control, makes the control of AC motors equivalent to that of separately excited DC motors by employing certain coordinate transformations and decoupling manipulations [1]. The control performance of sensorless field-oriented induction motors mainly relies on an accurate flux estimation. In practice, rotor fluxes are preferred to be estimated rather than directly measured. It is true that the inaccuracy of estimated fluxes causes a performance degradation of speed control. Current model (CM) and voltage model (VM) are two typical flux observers with the advantage of computation simplicity [2]. However, due to the sensitivity of parameter variations, CM and VM observers were respectively operated in low- and high-speed ranges [3]. The estimation accuracy and robustness of flux observers have attracted considerable attention in high performance induction drives. Using the measurements of stator currents and rotor speeds, a reduced-order flux observer

was utilized for the speed control of induction motors [4]. Hilairet et al. [5] proposed a two-stage extended Kalman filter for the flux and speed estimation of induction motors.

Variable structure systems with the sliding-mode (SM) method can offer some interesting features, including the robustness to parameters variations, insensitivity to disturbances and fast dynamics [7-9]. During the motion on a sliding surface, system responses are based on the derivative of the sliding surface that can result in an invariance property against uncertainties [10-12]. Moreover, the system trajectories in the integral sliding-mode (ISM) scheme can be established without a reaching phase, and the robustness subject to parameter variations and disturbances is guaranteed starting from the initial time instance [13-15]. Recently, the ISM method has been successfully applied to high-performance induction motor drives. For example, Hajian et al. [12] introduced a sliding-mode speed controller with two proportional-integral type sliding surfaces, in which an on-line search method was adopted to minimize the average real input power; In the work of Comanescu et al. [13], two ISM controllers were utilized to overcome the effect caused by the cross-coupling of d-q current dynamics. In order to obtain more accurate responses, the closed-loop framework was suggested to minimally rely upon the features of induction motors [14]. Besides, the computational complexity resulted from the iterative calculations between flux and speed estimations will degrade the control performance. Approaches of [12, 13] required the speed information and the rotor time constant of induction motors for flux estimates. The precision of flux estimation might be affected by the iterative calculations of estimated speeds and the variation of rotor time constants, which will consequently decrease the control performance of induction motors.

In most cases of sliding manifolds, a proportional-integral or proportional-derivative type sliding surface is adopted, where the order of integration or derivation is an integer. However, subject to the increasing system complexity, integer-order operators may be unable to meet the required performance and robustness of concern. There is a significant demand for a better flux estimation. The fractional calculus provides a possible approach due to the fact that the behaviors of many physical systems can be properly described by using the fractional-order system theory [15]. By adopting the concepts of fractional order calculus, it could have the advantages of adequate description of system dynamics, less sensitive to parameter variations, and reasonable realization by approximations [16, 17]. It was presented that the fractional order calculus could be applied to solving control problems and enhancing control performance [18]. Moreover, Podlubny [19] introduced the geometric and physical interpretations of fractional integration and differentiation. Compared with integer-order controllers, fractional order controllers can provide better responses regarding to external disturbances and parameter variations [20]. Applications of fractional order sliding-mode strategies have been widely addressed in different areas. For instance, Delavari et al. introduced a fractional-order PD^{α} surface sliding mode controller for a coupled second-order nonlinear system [21]; In the work of Calderón et al. [22], a fractional order sliding-mode control scheme was proposed to determine the switching surface of a DC/DC buck converter.

The accuracy of the flux estimation is sensible to the desired performance of field-oriented induction motors. It is motivated to provide a better formulation of the flux observer to achieve high-precision speed control. An ISM flux observer is introduced, where the estimated speed and the rotor time constant are not fed into the flux observer directly. Thus, this observer is insensitive to the errors in both speed estimation and rotor time constant. In this paper, a fractional-order integral sliding-mode (FOISM) flux observer is proposed for field-oriented induction motors. In the proposed scheme, the deviations between observed and measured stator currents are utilized to define the sliding surface. Accordingly, the FOISM control law is designed and the system convergence is

guaranteed by the Lyapunov theorem. Furthermore, a DSP/FPGA based experimental system is set up to evaluate the feasibility of proposed works.

The organization of this paper is as follows. Section 2 briefly describes the dynamic model of induction motors and the concepts of fractional order calculus. In addition, the approximation of fractional order operators and related numerical analyses are also represented. In Section 3, the design of a FOISM flux observer is addressed, in which the stability analysis based on the Lyapunov stability theorem is considered. Also, the speed estimation of the induction motor is discussed. Thereafter, simulations and experimental results are provided in Section 4 and Section 5, respectively. Finally, concluding remarks and future works are given in Section 6.

2. **Preliminaries.**

2.1. **Dynamic model of induction motors.**

It is noted that the mathematical model of a field-oriented induction motor is highly nonlinear. Based on the concept of vector control, the state equations of an induction motor in the stationary reference frame can be described as [23]

$$\begin{bmatrix} \dot{i}^s_{ds} \\ \dot{i}^s_{qs} \end{bmatrix} = k_1 \left(\begin{bmatrix} \eta & \omega_r \\ -\omega_r & \eta \end{bmatrix} \begin{bmatrix} \phi^s_{dr} \\ \phi^s_{qr} \end{bmatrix} - \eta L_m \begin{bmatrix} i^s_{ds} \\ i^s_{qs} \end{bmatrix} \right) - k_2 \begin{bmatrix} i^s_{ds} \\ i^s_{qs} \end{bmatrix} + k_3 \begin{bmatrix} v^s_{ds} \\ v^s_{qs} \end{bmatrix} \tag{1}$$

$$\begin{bmatrix} \dot{\phi}^s_{dr} \\ \dot{\phi}^s_{qr} \end{bmatrix} = - \left(\begin{bmatrix} \eta & \omega_r \\ -\omega_r & \eta \end{bmatrix} \begin{bmatrix} \phi^s_{dr} \\ \phi^s_{qr} \end{bmatrix} - \eta L_m \begin{bmatrix} i^s_{ds} \\ i^s_{qs} \end{bmatrix} \right) \tag{2}$$

where $k_1 = \frac{k_3 L_m}{L_r}$, $k_2 = \frac{R_s}{\sigma L_s}$, $k_3 = \frac{1}{\sigma L_s}$ and $\eta = \frac{R_r}{L_r}$. In (1) and (2), i, ϕ, v, R and L are the current, flux, voltage, resistance and inductance, the superscript s means the component in the stationary reference frame, subscripts d and q denote components of d- and q-axis, subscripts r and s mean the rotor and stator. In addition, L_m is the mutual inductance between the rotor and stator, σ is the total flux leakage coefficient, and ω_r is the electrical angular speed of the rotor, respectively.

2.2. **Fractional order calculus.**

Fractional order calculus, developed from ordinary calculus, is a generalization of the integration and differentiation to the non-integer (fractional) order generalized operator ${}_aD^q_t$, in which a and t are limits and q is the order of the operator. This operator is a notation for both the fractional derivative and the fractional integral in a single expression, which can be represented as follows [15, 24]:

$${}_aD^q_t = \begin{cases} \dfrac{d^q}{dt^q}, & q > 0 \\ 1, & q = 0 \\ \int_a^t (d\tau)^{-q}, & q < 0 \end{cases} \tag{3}$$

Two general fractional order integral/differential operations are commonly discussed, Caputo and Riemann-Liouville (R-L) fractional operators. Physically, the R-L fractional operator has initial value problems [25]. Therefore, the Caputo fractional operator is more practical than the R-L one. In this work, the Caputo fractional operator is adopted for system modeling and analyzing, in which the fractional order differential equation of $f(t)$ is defined as follows:

$${}_aD^q_t f(t) = \frac{1}{\Gamma(m-q)} \int_a^t \frac{f^{(m)}(\tau)}{(t-\tau)^{q+1-m}} d\tau, \quad \forall\, 0 \le m-1 < q \le m,\ m \in \mathcal{N} \tag{4}$$

where $\Gamma(\bullet)$ is the Euler's gamma function, and m is the first integer which is not less than q. The Laplace transform of the Caputo differential equation can be described in the following

$$\mathcal{L}\left\{{}_0D_t^q f(t)\right\} = s^q F(s) - \sum_{k=0}^{m-1} s^{m-1-k} f^{(k)}(0). \tag{5}$$

In (5), it is observed that only integer-order operators are involved in the derivative of function $f(t)$ at the initial point. Without loss of generality, the initial state and input of system dynamics are considered as zeros. Therefore, the Laplace transformation of the Caputo differential equation for zero initial conditions with a fractional order λ can be rewritten as follows:

$$\mathcal{L}\left\{{}_0D_t^\lambda f(t)\right\} = s^\lambda F(s) \tag{6}$$

where $0 < \lambda \leq 1$. Intuitively, the fractional-order modeling can give a more adequate description of complex system features, and then a better performance can be obtained with a proper choice of orders. In the rest of this paper, a simplified notation D^λ is utilized to represent the fractional order operator, $D^\lambda \equiv {}_0D_t^\lambda$.

2.3. **Approximation of fractional operators.** For practical realizations, transfer functions with fractional order integral/differential operators are usually approximated by integer-order transfer functions, in which a close enough behavior is acquired with less complexity. Referring to [22], the implementations of fractional order controllers can be categorized into two approaches, the analog approximation and the digital approximation.

For example, let $[\omega_A, \omega_B]$ be the frequency range of concern. To obtain a proper approximation of a fractional order differential operator, high- and low-transitional frequencies are chosen as $\omega_h \gg \omega_B$ and $\omega_l \ll \omega_A$, respectively. Then, the approximation of a frequency-band fractional order differential operator can be determined as [26, 27]

$$s^\lambda \approx \left(\frac{\omega_u}{\omega_h}\right)^\lambda \prod_{k=-N}^{N} \frac{1 + s/\omega_k^{'}}{1 + s/\omega_k} \tag{7}$$

$$\omega_k^{'} = \omega_l \left(\frac{\omega_h}{\omega_l}\right)^{\frac{k+N+1/2-\lambda/2}{2N+1}}, \quad \omega_k = \omega_l \left(\frac{\omega_h}{\omega_l}\right)^{\frac{k+N+1/2+\lambda/2}{2N+1}}$$

where $\omega_k^{'}$ is the zero of rank k, ω_k is the pole of rank k, $2N+1$ is the number of zeros and poles, $\omega_u = (\omega_l \cdot \omega_h)^{1/2}$ and $\lambda > 0$. Similarly, the case of $\lambda < 0$ can be dealt with by swapping the numerator and denominator of (7).

2.4. **Numerical analyses of fractional order operators.** In this paper, a FOISM flux observer is approximately formulated with a bounded-frequency transfer function. In practice, the approximate transformations of fractional order operators are related to a frequency truncation. Intuitively, the degree of approximation of a fractional order operator is related to chosen transitional frequencies and the order N. It can be expected that a better approximation can be obtained with a larger N. However, the computation complexity will be increased with the increasing of N. On the other hand, with a fixed N, characteristics related to chosen bounded frequencies are also interested. In this study, both fractional order integral and differential operators are contributed to sliding-mode control actions. Therefore, the approximation of fractional order operators with different parameter settings is worthy of further investigation. Without loss of generality, the transfer function $s^{-\lambda} + s^{-\lambda+1}$, $\lambda = 0.5$ is selected to discuss the approximate modeling. With $N = 3$, high- and low-transitional frequencies are respectively selected as:
1) Case 1: $\omega_h = 10^2\ rad/sec$ and $\omega_l = 10^{-2}\ rad/sec$,

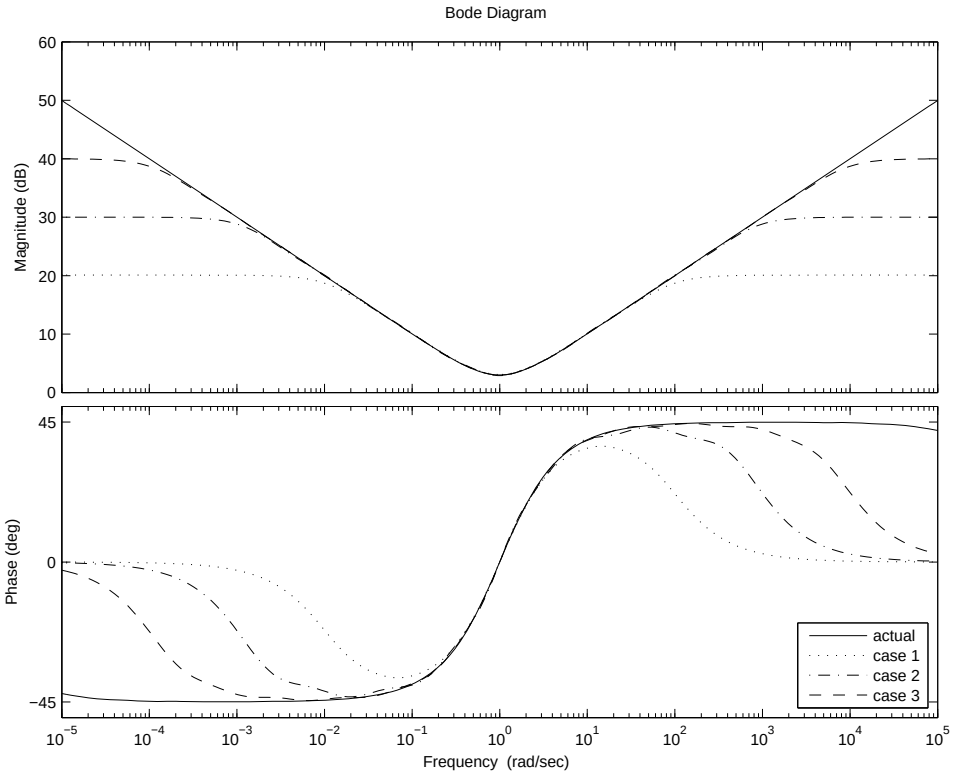

FIGURE 1. Frequency responses of the approximations to the transfer function $s^{-0.5} + s^{0.5}$ with different transitional frequencies

2) Case 2: $\omega_h = 10^3\ rad/sec$ and $\omega_l = 10^{-3}\ rad/sec$,
3) Case 3: $\omega_h = 10^4\ rad/sec$ and $\omega_l = 10^{-4}\ rad/sec$.

From (7), the approximate transfer functions of the fractional operator $s^{0.5}$ corresponding to aforementioned cases are summarized in Table 1. It is noticed that the approximate transfer function of $s^{-0.5}$ is the inverse function of $s^{0.5}$. Frequency responses of the approximate transfer functions of $s^{-0.5} + s^{0.5}$ with different transitional frequencies are depicted in Figure 1. It can be seen that there exist significant approximation errors outside the selected range transitional frequencies. Thus, to obtain a better approximation in the viewpoint of frequency responses, a wider range of $[\omega_l, \omega_h]$ is adopted. In this paper, the induction motor is driven by a sinusoidal pulse-width modulation (SPWM) inverter of which the switching frequency is 10 kHz. Regarding to the switching frequency, the transitional frequencies for the approximation of integral/differential operators are set to $\omega_h = 10^4\ rad/sec$ and $\omega_l = 10^{-4}\ rad/sec$.

Remark 2.1. *Certain approximations can be obtained with selected high- and low-transitional frequencies. With regard to the feasibility of implementation and the accuracy of approximation, the transitional frequency range needs to be selected adequately according to the characteristics of controlled plants.*

3. **Flux and Speed Estimation.** From (1) and (2), the conventional sliding-mode current model flux observer can be represented as follows [28]:

$$\begin{bmatrix} \dot{\hat{i}}^s_{ds} \\ \dot{\hat{i}}^s_{qs} \end{bmatrix} = k_1 \begin{bmatrix} \psi_d \\ \psi_q \end{bmatrix} - k_2 \begin{bmatrix} \hat{i}^s_{ds} \\ \hat{i}^s_{qs} \end{bmatrix} + k_3 \begin{bmatrix} v^s_{ds} \\ v^s_{qs} \end{bmatrix} \tag{8}$$

TABLE 1. Approximations of $s^{0.5}$ with various transitional frequencies

Case 1: $s^{0.5} \approx \frac{0.1(1+s/0.0139)(1+s/0.0518)(1+s/0.1931)(1+s/0.7197)(1+s/2.6827)(1+s/10.0000)(1+s/37.2759)}{(1+s/0.0268)(1+s/0.1000)(1+s/0.3728)(1+s/1.3895)(1+s/5.1795)(1+s/19.3070)(1+s/71.9686)}$
Case 2: $s^{0.5} \approx \frac{0.0316(1+s/0.0016)(1+s/0.0118)(1+s/0.0848)(1+s/0.6105)(1+s/4.9340)(1+s/3.6228)(1+s/227.5846)}{(1+s/0.0044)(1+s/0.0316)(1+s/0.2276)(1+s/1.6379)(1+s/11.7877)(1+s/84.8343)(1+s/610.5402)}$
Case 3: $s^{0.5} \approx \frac{0.01(1+s/0.0002)(1+s/0.0027)(1+s/0.0373)(1+s/0.5179)(1+s/7.1969)(1+s/100.0000)(1+s/1389.4955)}{(1+s/0.0007)(1+s/0.0100)(1+s/0.1389)(1+s/1.9307)(1+s/26.8269)(1+s/372.7594)(1+s/5179.4747)}$

$$\begin{bmatrix} \dot{\hat{\phi}}^s_{dr} \\ \dot{\hat{\phi}}^s_{qr} \end{bmatrix} = - \begin{bmatrix} \psi_d \\ \psi_q \end{bmatrix} \tag{9}$$

in which terms ψ_d and ψ_q can be obtained as

$$\begin{bmatrix} \psi_d \\ \psi_q \end{bmatrix} = \begin{bmatrix} \eta & \omega_r \\ -\omega_r & \eta \end{bmatrix} \begin{bmatrix} \hat{\phi}^s_{dr} \\ \hat{\phi}^s_{qr} \end{bmatrix} - \eta L_m \begin{bmatrix} \hat{i}_{ds} \\ \hat{i}_{qs} \end{bmatrix} \tag{10}$$

Referring to (2), (9) and (10), it can be seen that the flux estimation could be affected by parameter variations of R_r and L_r. In this paper, a FOISM observer is proposed to improve the performance of flux estimation. Based on the current errors, $\tilde{i}^s_d = \hat{i}^s_{ds} - i^s_{ds}$, $\tilde{i}^s_q = \hat{i}^s_{qs} - i^s_{qs}$, between measured and estimated stator currents, the sliding surface of the FOISM flux observer is defined as

$$\mathbf{S} = \begin{bmatrix} s_d \\ s_q \end{bmatrix} = \begin{bmatrix} c_1 \tilde{i}^s_d + c_2 D^{-\lambda} \tilde{i}^s_d \\ c_1 \tilde{i}^s_q + c_2 D^{-\lambda} \tilde{i}^s_q \end{bmatrix} \tag{11}$$

where c_1 and c_2 are positive constants. In (11), $D^{-\lambda}$ is considered as a fractional order integral operator with $\lambda \in (0, 1]$. From (10) and (11), the derivative of $\mathbf{S}$ can be derived as follows:

$$\begin{aligned} \dot{\mathbf{S}} &= c_1 \begin{bmatrix} \dot{\hat{i}}^s_{ds} - \dot{i}^s_{ds} \\ \dot{\hat{i}}^s_{qs} - \dot{i}^s_{qs} \end{bmatrix} + c_2 D^{-\lambda+1} \begin{bmatrix} \tilde{i}^s_d \\ \tilde{i}^s_q \end{bmatrix} \\ &= c_1 k_1 \begin{bmatrix} \psi_d \\ \psi_q \end{bmatrix} + c_1 k_1 \begin{bmatrix} M \\ N \end{bmatrix} - c_1 k_2 \begin{bmatrix} \tilde{i}^s_d \\ \tilde{i}^s_q \end{bmatrix} + c_2 D^{-\lambda+1} \begin{bmatrix} \tilde{i}^s_d \\ \tilde{i}^s_q \end{bmatrix} \end{aligned} \tag{12}$$

where $M = -\eta \phi^s_{dr} - \omega_r \phi^s_{qr} + \eta L_m i^s_d$, $N = \omega_r \phi^s_{dr} - \eta \phi^s_{qr} + \eta L_m i^s_q$, and M, N are predetermined based on the rated rotor speed, electrical parameters and the reference values of rotor fluxes. Derivations of ψ_d and ψ_q are discussed in the following. Let $V = \frac{1}{2}\mathbf{S}^T\mathbf{S}$ be a Lyapunov function candidate. Then the derivative of V can be obtained as follows

$$\begin{aligned} \dot{V} &= \mathbf{S}^T \dot{\mathbf{S}} \\ &= \mathbf{S}^T \left\{ c_1 k_1 \begin{bmatrix} \psi_d \\ \psi_q \end{bmatrix} + c_1 k_1 \begin{bmatrix} M \\ N \end{bmatrix} - c_1 k_2 \begin{bmatrix} \tilde{i}^s_d \\ \tilde{i}^s_q \end{bmatrix} + c_2 D^{-\lambda+1} \begin{bmatrix} \tilde{i}^s_d \\ \tilde{i}^s_q \end{bmatrix} \right\} \end{aligned} \tag{13}$$

Assume that $\max|c_1 k_1 M| < Q_d < \infty$ and $\max|c_1 k_1 N| < Q_q < \infty$. It can be obtained that $s_d \cdot \max|c_1 k_1 M| < s_d \cdot sign(s_d) Q_d$ and $s_q \cdot \max|c_1 k_1 N| < s_q \cdot sign(s_q) Q_q$. Thus (13) can be rewritten as

$$\dot{V} < \mathbf{S}^T \left\{ c_1 k_1 \begin{bmatrix} \psi_d \\ \psi_q \end{bmatrix} - c_1 k_2 \begin{bmatrix} \tilde{i}^s_d \\ \tilde{i}^s_q \end{bmatrix} + c_2 D^{-\lambda+1} \begin{bmatrix} \tilde{i}^s_d \\ \tilde{i}^s_q \end{bmatrix} + \begin{bmatrix} sign(s_d) Q_d \\ sign(s_q) Q_q \end{bmatrix} \right\} \tag{14}$$

From (14), the stabilizing control law can be determined as

$$\begin{bmatrix} \psi_d \\ \psi_q \end{bmatrix} = \frac{k_2}{k_1} \begin{bmatrix} \tilde{i}^s_d \\ \tilde{i}^s_q \end{bmatrix} - \frac{u_0}{c_1 k_1} \begin{bmatrix} sign(s_d) \\ sign(s_q) \end{bmatrix} - \frac{c_2}{c_1 k_1} D^{-\lambda+1} \begin{bmatrix} \tilde{i}^s_d \\ \tilde{i}^s_q \end{bmatrix} \tag{15}$$

where

$$sign(s_j) = \begin{cases} s_j/|s_j|, & \text{if } s_j \neq 0 \\ 0, & \text{otherwise} \end{cases}$$

$j \in \{d, q\}$ and u_0 is a positive constant gain.

Theorem 3.1. *The sliding mode of an induction motor using the proposed FOISM flux observer is guaranteed if the constant gain u_0 of the control law (15) is satisfied with $u_0 > \max[Q_d, Q_q]$.*

Proof: Substituting ψ_d and ψ_q of (15) into (14), it gives that

$$\begin{aligned} \dot{V} &\leq \begin{bmatrix} s_d \\ s_q \end{bmatrix}^T \left(- \begin{bmatrix} u_0 \cdot sign(s_d) \\ u_0 \cdot sign(s_q) \end{bmatrix} + \begin{bmatrix} sign(s_d) Q_d \\ sign(s_q) Q_q \end{bmatrix} \right) \\ &= - \left[s_d \cdot sign(s_d)(u_0 - Q_d) + s_q \cdot sign(s_q)(u_0 - Q_q) \right] \end{aligned}$$

By the assumption $u_0 > \max[Q_d, Q_q]$, it can be obtained that $u_0 - Q_d > 0$ and $u_0 - Q_q > 0$. Also, it is noted that $s_d \cdot sign(s_d) \geq 0$ and $s_q \cdot sign(s_q) \geq 0$. Therefore, we can conclude that $\dot{V} \leq 0$, and the sliding mode of the FOISM flux estimation is guaranteed. □

In summary, the convergence of the flux observer can be ensured by selecting a large enough u_0 subject to $u_0 > \max[Q_d, Q_q]$. However, an excessively large u_0 may produce a high control signal that could result in saturated driving. When system trajectories reach to the sliding surface, i.e., $\mathbf{S} = [0, 0]^T$, d- and q-axis observed currents will converge to actual currents. Accordingly, errors of flux estimation will also tend to zeros.

It is well known that the sliding-mode method suffers from the problem of chattering, which can excite unexpected high frequency responses. In this paper, a saturation function is adopted to eliminate the chattering effect as follows [29]:

$$sat(s_j) = \begin{cases} sign(s_j/\varepsilon), & \text{if } |s_j/\varepsilon| \geq 1 \\ s_j/\varepsilon, & \text{if } |s_j/\varepsilon| < 1 \end{cases}, \; j \in \{d, q\} \tag{16}$$

where $\varepsilon > 0$ represents the thickness of the boundary layer, as shown in Figure 2. From (15) and (16), the FOISM flux observer with a saturation function can be described as follows:

$$\begin{bmatrix} \psi_d \\ \psi_q \end{bmatrix} = \begin{bmatrix} -\frac{1}{c_1 k_1} u_0 \cdot sat(s_d) + \frac{k_2}{k_1} \tilde{i}_d^s - \frac{c_2}{c_1 k_1} D^{-\lambda+1} \tilde{i}_d^s \\ -\frac{1}{c_1 k_1} u_0 \cdot sat(s_q) + \frac{k_2}{k_1} \tilde{i}_q^s - \frac{c_2}{c_1 k_1} D^{-\lambda+1} \tilde{i}_q^s \end{bmatrix} \tag{17}$$

Remark 3.1. *The integral sliding-mode (ISM) flux observer can be considered as a special case of the proposed FOISM flux observer, in which λ is set to 1.*

Remark 3.2. *All the terms associated with the speed and rotor time constant are embedded in restrictive and bounded terms, which are replaced by a constant gain. The rotor speed and time constant are not fed into the flux observer directly, that makes the flux estimation insensitive to the iterative calculations of the estimated speed and the variations of the rotor time constant of induction motors.*

Remark 3.3. *Given $0 < \lambda \leq 1$, it can be obtained that $-\lambda + 1 \in [0, 1)$. Thus, from (17), the proposed control actions consist of fractional order differential terms. In fact, both operations of fractional order integral and differential operators are embedded in control actions, where integral terms are inherited in sliding surfaces, s_d and s_q.*

The estimated rotor speed of an induction motor is derived from the flux estimation. From (10), the speed estimation can be obtained in the following:

$$\begin{bmatrix} \psi_d \\ \psi_q \end{bmatrix} = \begin{bmatrix} \eta & \hat{\omega}_r \\ -\hat{\omega}_r & \eta \end{bmatrix} \begin{bmatrix} \hat{\phi}_{dr}^s \\ \hat{\phi}_{qr}^s \end{bmatrix} - \eta L_m \begin{bmatrix} \hat{i}_{ds}^s \\ \hat{i}_{qs}^s \end{bmatrix} \tag{18}$$

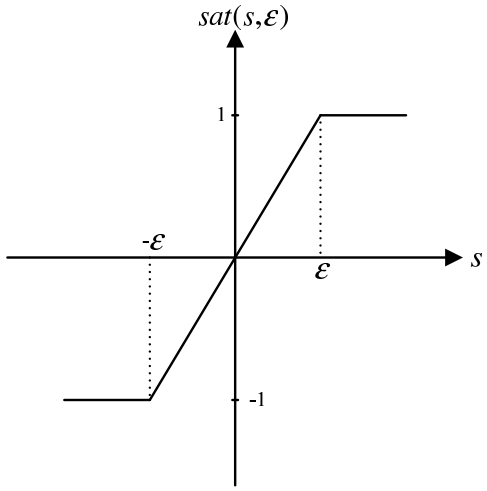

FIGURE 2. The diagram of the saturation function

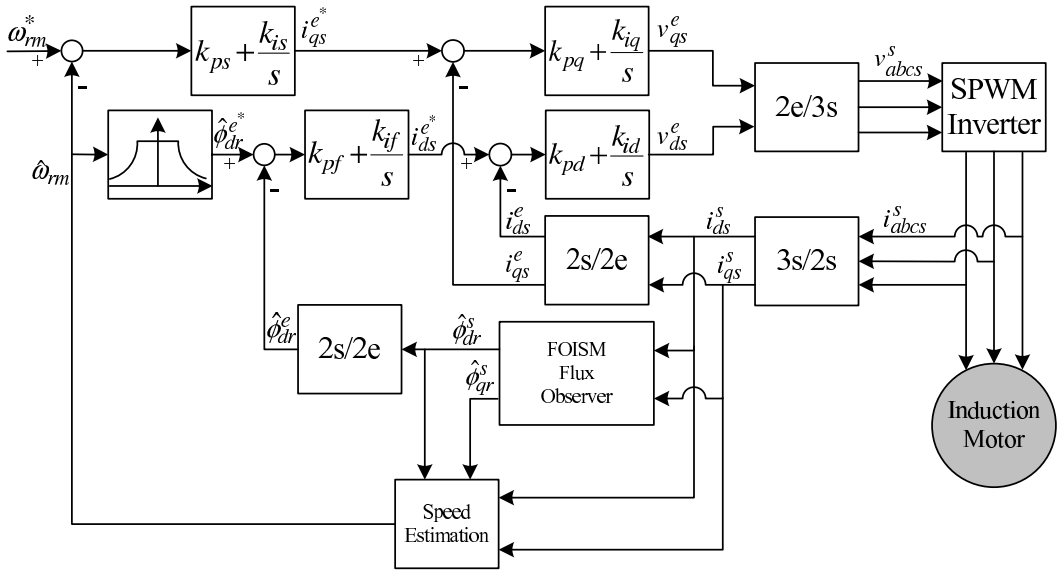

FIGURE 3. The block diagram of the proposed scheme

From (18), the estimated speed of an induction motor can be described as follows:

$$\hat{\omega}_r = \frac{\hat{\phi}^s_{qr}\psi_d - \hat{\phi}^s_{dr}\psi_q - \eta L_m\left(\hat{i}^s_{qs}\hat{\phi}^s_{dr} - \hat{i}^s_{ds}\hat{\phi}^s_{qr}\right)}{\left(\hat{\phi}^s_{dr}\right)^2 + \left(\hat{\phi}^s_{qr}\right)^2} \tag{19}$$

$$\hat{\omega}_{rm} = \frac{2}{N_p}\hat{\omega}_r \tag{20}$$

where N_p is the number of poles and $\hat{\omega}_{rm}$ is the estimated mechanical angular speed of the rotor. Consequently, the block diagram for a sensorless field-oriented induction motor with the proposed FOISM flux observer is depicted in Figure 3, where the superscript e denotes components in the reference coordinate frame of the rotor flux.

4. **Simulation Results.** In this paper, a three-phase 0.1 kW squirrel cage induction machine is used, whose parameters are shown in Table 2. Simulations are performed in Matlab to validate the performance of the proposed FOISM observer. Four types

TABLE 2. Parameters of the induction motor

Parameter	R_s (Ω)	J ($\mathrm{kg}\cdot\mathrm{m}^2$)	N_p	L_r (H)	rated current (A)	rated speed (rpm)
Value	28.72	0.0001	2	0.7262	1.05	3000
Parameter	R_r (Ω)	B ($\mathrm{m/rad}\cdot\mathrm{s}$)	L_s (H)	L_m (H)	rated voltage (V)	
Value	15.89	0.000692	0.7262	0.6817	105	

TABLE 3. Speed command evolution [30]

Time interval	Speed commands
$0-0.5$	The speed command starts from zero at $t=0$ s.
$0.5-5$	A step command, 900 rpm, is applied at $t=0.5$ s.
$5-8$	A speed command starts from 900 rpm to 720 rpm at $t=5$ s.
$8-11$	A speed command starts from 720 rpm to 1080 rpm at $t=8$ s.
$11-14$	A constant speed command of 900 rpm is applied at $t=11$ s.
$14-17.14$	A sine function $180*\sin(2t)$ is added to the previous constant speed command at $t=14$ s.
$17.14-20$	The speed command of 900 rpm is kept in the rest time of the simulaution.

of flux observers, CM [2], SM [28], ISM [12] and FOISM, are considered, in which the speed, flux and current controllers will remain identically. Following the proposed design procedures, the coefficients of related controllers and observers are summarized in Table 4. To verify the superiority of the proposed FOISM observer, various speed commands are applied while keeping a constant nominal load torque at 0.3 Nt-m. The step, increased/decreased and sine wave speed commands are applied and specified in Table 3 [30], in which steady-state, transient and tracking responses of presented flux observers can be revealed. Simulation results of aforementioned observers are shown in Figures 4-7, in which the speed response, speed error, rotor flux and q-axis current error are depicted. It is noted that the FOISM observer can provide a better flux response than other observers. Furthermore, the consequently speed tracking regarding to the proposed FOISM observer is more accurate than the other mentioned observers. Also, the performance validations of speed and flux control can be indicated by the convergences of the speed and q-axis current.

5. **Experimental Results.** In this paper, control responses of flux and speed tracking are mainly addressed, where flux observers are utilized in the presence of different speed commands and load conditions. Experimental results are presented by calculating the root-mean-square (RMS) values of tracking errors. As shown in Figure 8, a DSP and FPGA based experimental system with a sampling period of 1 ms is set up to validate proposed results. In the experimental platform, the TMS320C6713 DSP board is used to implement all control algorithms coded with C language and the Stratix EP1S25 FPGA board is used to implement all functions of data bus, encoder, A/D converter and SPWM inverter. The induction motor is a Nikki Denso NF21-3F three-phase squirrel cage machine (parameters have been given in Table 2). Currents are measured by using Hall sensors. The external load torque is produced by a Mitsubishi ZKG-10AN powder clutch. Coefficients of relative controllers and observers are the same as simulation, which have been provided in Table 4. To highlight the feasibility and superiority of the proposed control scheme, forward-reverse operations are implemented to validate the capability of dealing with load disturbance, where extrogenous loads are applied on $t=3$, 13, 23, 33

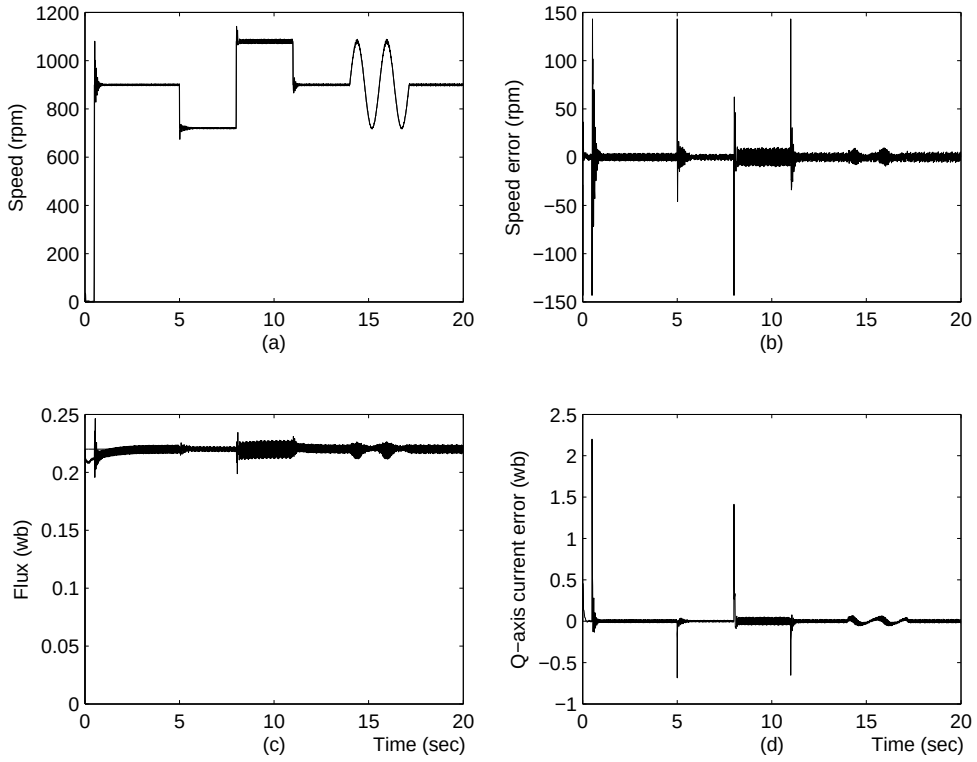

FIGURE 4. Simulation results corresponding to the CM flux observer: (a) speed response, (b) speed error, (c) rotor flux, (d) q-axis current error

second and removed on $t = 7$, 17, 27, 37 second. In the meantime, the flux and load torque commands are set to 0.22 wb and 0.3 Nt-m, respectively. Some of the control responses of CM [2], SM [28], ISM [12] and FOISM flux observers on $\omega_{rm}^* = 1800$ rpm are illustrated in Figures 9-12, including estimations of the rotor speed, estimations of d-axis flux, the errors of d- and q-axis currents, and control efforts of d- and q-axes, respectively. From these experimental results, it is apparent that d- and q-axis chatting phenomena and current errors of the FOISM flux observer are smaller than counterparts of CM, SM and ISM methods. Furthermore, the proposed flux observer can provide a better tracking accuracy of d- and q-axis flux estimations and consequent speed responses. About the experimental results, it is noted that a better tracking performance of field-oriented induction motors can be established if the accurate flux estimation is provided. With regard to different speed commands, 500, 900 and 1800 rpm, transient responses of the speed control with different load conditions are shown in Figures 13 and 14. It can be observed that the instant speed error and recovery time of the FOISM flux observer are the smallest among four estimation methods subject to load disturbances. Moreover, the steady-state responses of speed and flux tracking are illustrated in Figures 15 and 16, respectively. It is obvious that speed and flux tracking errors with the FOISM flux observer are less than counterparts of other observers. From Figures 13-16, it can be summarized that the proposed FOISM flux observer can provide much better control responses in both transient and steady-state manners with various speed commands and extrogenous loads.

6. **Conclusions.** In this paper, an induction machine based on the sensorless field-oriented control scheme is discussed, where the flux/speed estimation and tracking are main subjects of concern. A fractional order integral sliding-mode flux observer is proposed to take the advantage of the flexibility of fractional orders, in which the superiority

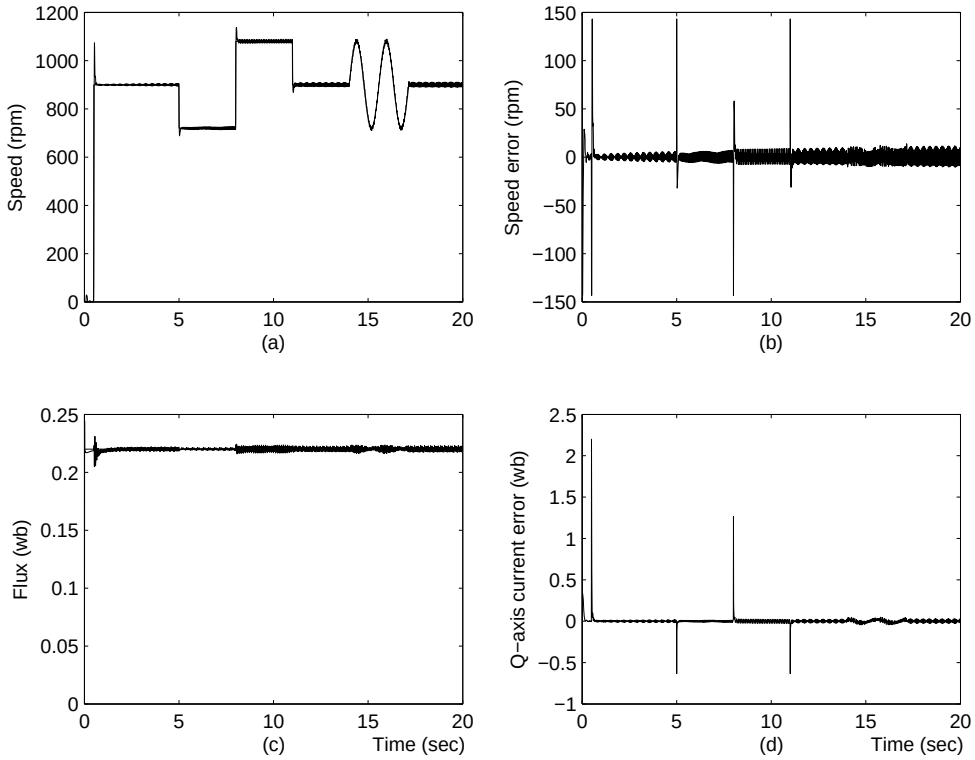

FIGURE 5. Simulation results corresponding to the SM flux observer: (a) speed response, (b) speed error, (c) rotor flux, (d) q-axis current error

TABLE 4. Coefficients of controllers and observers

Coefficient	k_{pd}	k_{id}	k_{pq}	k_{iq}	k_{pf}	k_{if}
Value	65	1200	45	4000	30	100
Coefficient	k_{ps}	k_{is}	c_1	c_2	u_0	λ
Value	0.08	0.05	1	5	1000	0.5

is verified by numerical analyses. Furthermore, the associated performance of speed control is investigated. A DSP/FPGA based experimental system is set up to validate the feasibility of proposed works. Compared with integer-order flux observers, simulation and experimental results illustrate that the proposed FOISM flux observer can achieve much better performance in both steady-state and transient responses subject to load disturbances. It is observed that the use of fractional-order schemes can provide better responses compared with the counterparts of integer-order approaches. Also, the tracking performance of vector-controlled induction motors is getting better if a relatively robust and accurate flux observer is provided. On the other hand, the flux estimation is based on that the orders of integral/differential operators are pre-determined. Given with certain orders, the feasibility of the proposed results has been evaluated with experimental implementations. In practice, there could be a better choice for the orders of fractional operators, and then the control performance can be further improved. Thus, deriving an adaptive law to determine optimized fractional orders is a promising challenge.

REFERENCES

[1] Y.-H. Chang, Y.-Y. Wang, M.-H. Hung and P.-C. Chen, Regional stability and H_∞ performance control of an input-saturated induction motor via LMI approach, *Asian Journal of Control*, vol.7, no.4, pp.368-379, 2005.

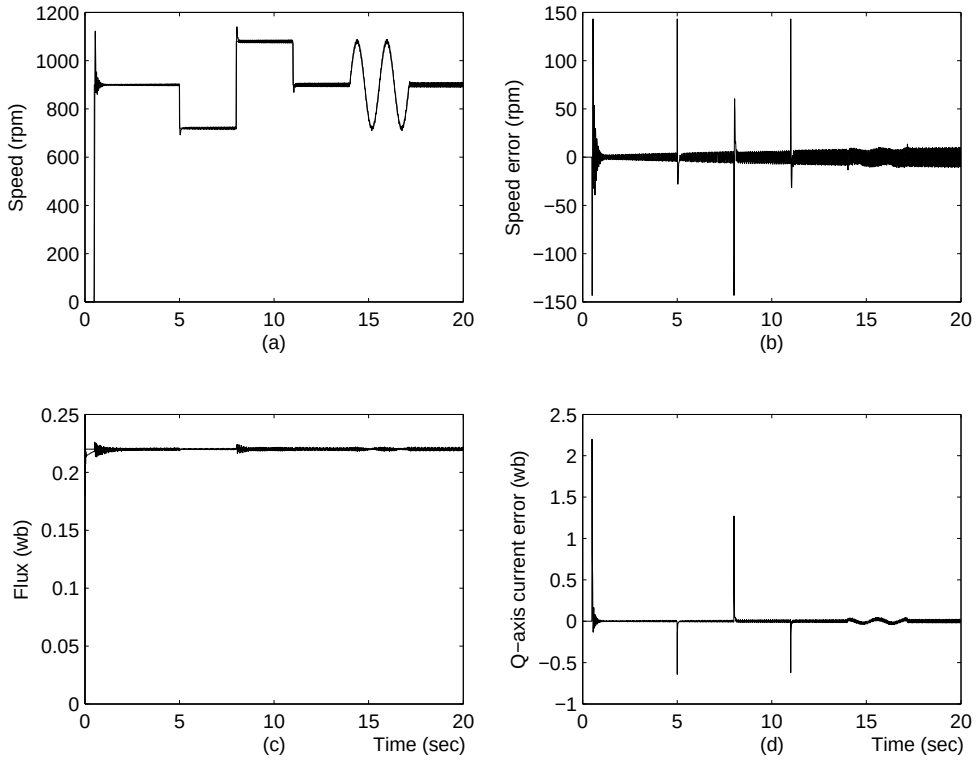

FIGURE 6. Simulation results corresponding to the ISM flux observer: (a) speed response, (b) speed error, (c) rotor flux, (d) q-axis current error

[2] P. L. Jansen and R. D. Lorenz, A physically insightful approach to the design and accuracy assessment of flux observers for field oriented induction machine drives, *IEEE Trans. on Industry Applications*, vol.30, no.1, pp.101-109, 1994.

[3] Y.-H. Chang, C.-I Wu, H.-W. Lin and N.-D. Kuo, Robust performance control of vector-controlled induction motors with gain-scheduled estimation and input-output linearization, *International Journal of Innovative Computing, Information and Control*, vol.7, no.1, pp.269-288, 2011.

[4] F. Alonge and F. D'Ippolito, Design and sensitivity analysis of a reduced-order rotor flux optimal observer for induction motor control, *Control Engineering Practice*, vol.15, no.12, pp.1508-1519, 2007.

[5] M. Hilairet, F. Auger and E. Berthelot, Speed and rotor flux estimation of induction machines using a two-stage extended Kalman filter, *Automatica*, vol.45, no.8, pp.1819-1827, 2009.

[6] K. D. Young, V. I. Utkin and Ü. Özgüner, A control engineer's guide to sliding mode control, *IEEE Trans. on Control Systems Technology*, vol.7, no.3, pp.328-342, 1999.

[7] V. I. Utkin, J. Guldner and J. Shi, *Sliding Mode Control in Electro-Mechanical Systems*, CRC Press, Taylor & Francis Group, Boca Raton, FL, 2009.

[8] C.-Y. Chen, Sliding mode controller design of induction motor based on space-vector pulsewidth modulation method, *International Journal of Innovative Computing, Information and Control*, vol.5, no.10(B), pp.3603-3614, 2009.

[9] V. I. Utkin and J. Shi, Integral sliding mode in systems operating under uncertainty conditions, *Proc. of the 35th Conference on Decision and Control*, Kobe, Japan, pp.4591-4596, 1996.

[10] J. Lian, J. Zhao and G. M. Dimirovski, Model reference adaptive integral sliding mode control for switched delay systems, *International Journal of Innovative Computing, Information and Control*, vol.4, no.8, pp.2025-2032, 2008.

[11] M. Jiménez-Lizárraga and L. Fridman, Robust Nash strategies based on integral sliding mode control for a two players uncertain linear affine-quadratic game, *International Journal of Innovative Computing, Information and Control*, vol.5, no.2, pp.241-251, 2009.

[12] M. Hajian, G. R. Arab Markadeh, J. Soltani and S. Hoseinnia, Energy optimized sliding-mode control of sensorless induction motor drives, *Energy Conversion and Management*, vol.50, no.9, pp.2296-2306, 2009.

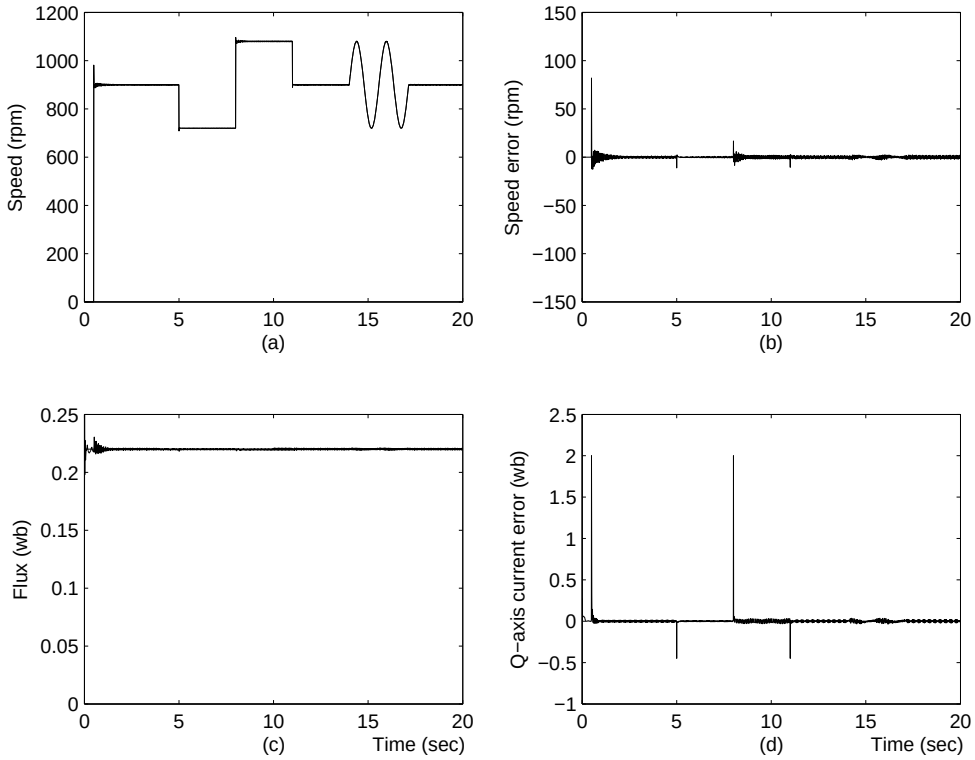

FIGURE 7. Simulation results corresponding to the FOISM flux observer: (a) speed response, (b) speed error, (c) rotor flux, (d) q-axis current error

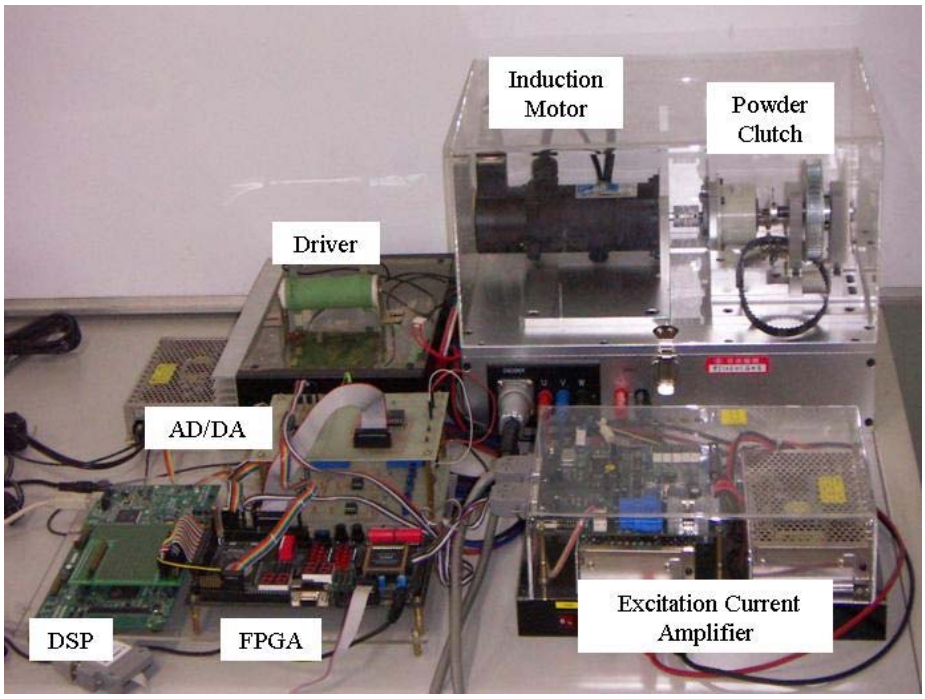

FIGURE 8. The experimental system setup

[13] M. Comanescu, L. Xu and T. D. Batzel, Decoupled current control of sensorless induction-motor drives by integral sliding mode, *IEEE Trans. on Industrial Electronics*, vol.55, no.11, pp.3836-3845, 2008.

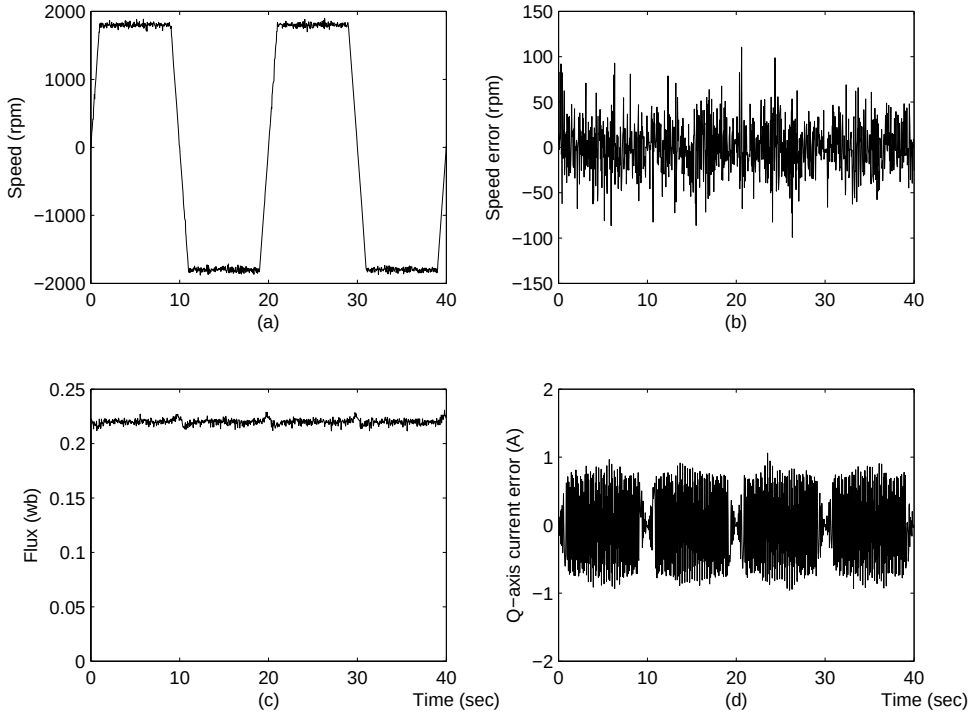

FIGURE 9. Simulation results corresponding to the CM flux observer on $\omega_{rm}^{*} = 1800$ rpm: (a) speed response, (b) speed error, (c) rotor flux, (d) q-axis current error

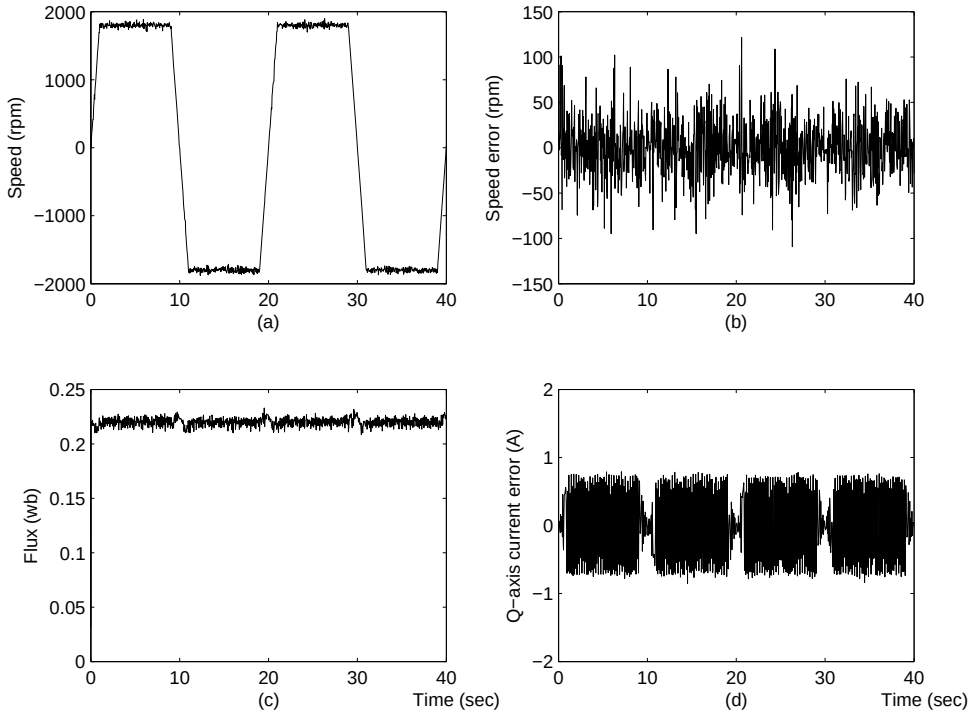

FIGURE 10. Experimental responses corresponding to the SM flux observer on $\omega_{rm}^{*} = 1800$ rpm: (a) speed response, (b) speed error, (c) rotor flux, (d) q-axis current error

[14] F. Jadot, F. Malrait, F. Moreno-Valenzuela and R. Sepulchre, Adaptive regulation of vector-controlled induction motors, *IEEE Trans. on Control Systems Technology*, vol.17, no.3, pp.646-657, 2009.

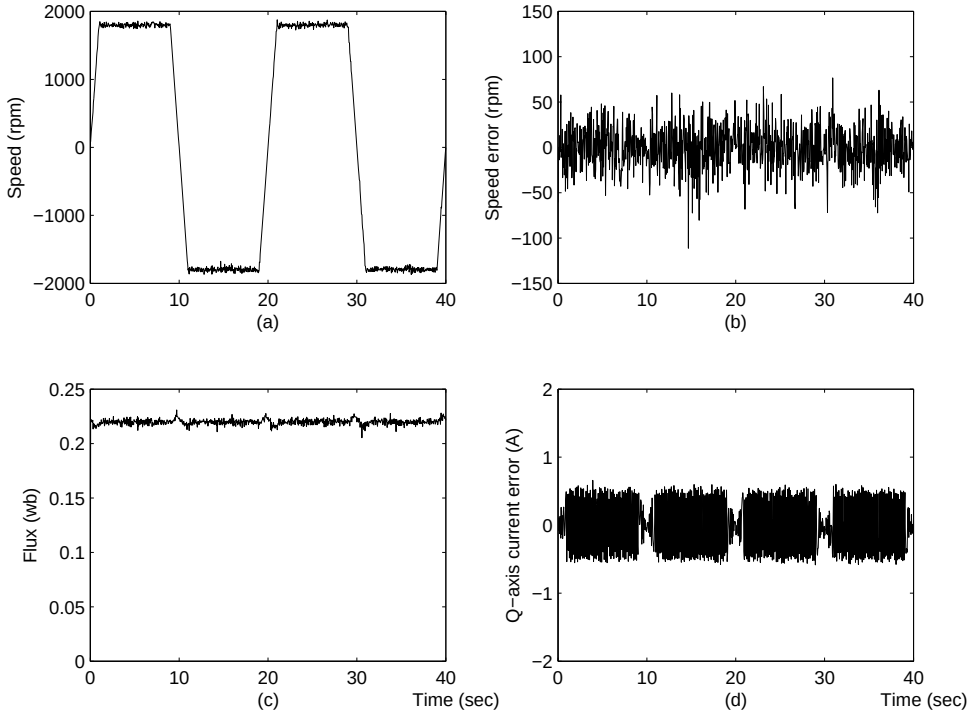

FIGURE 11. Experimental responses corresponding to the ISM flux observer on $\omega_{rm}^{*} = 1800$ rpm: (a) speed response, (b) speed error, (c) rotor flux, (d) q-axis current error

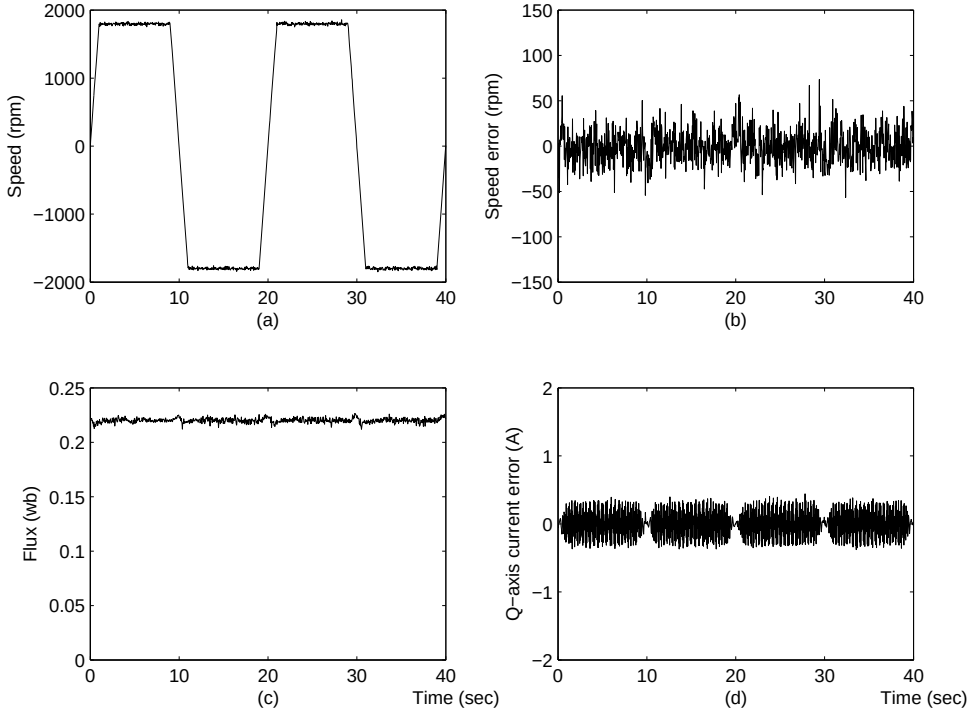

FIGURE 12. Experimental responses corresponding to the FOISM flux observer on $\omega_{rm}^{*} = 1800$ rpm: (a) speed response, (b) speed error, (c) rotor flux, (d) q-axis current error

[15] M. S. Tavazoei and M. Haeri, A note on the stability of fractional order systems, *Mathematics and Computers in Simulation*, vol.79, no.5, pp.1566-1576, 2009.

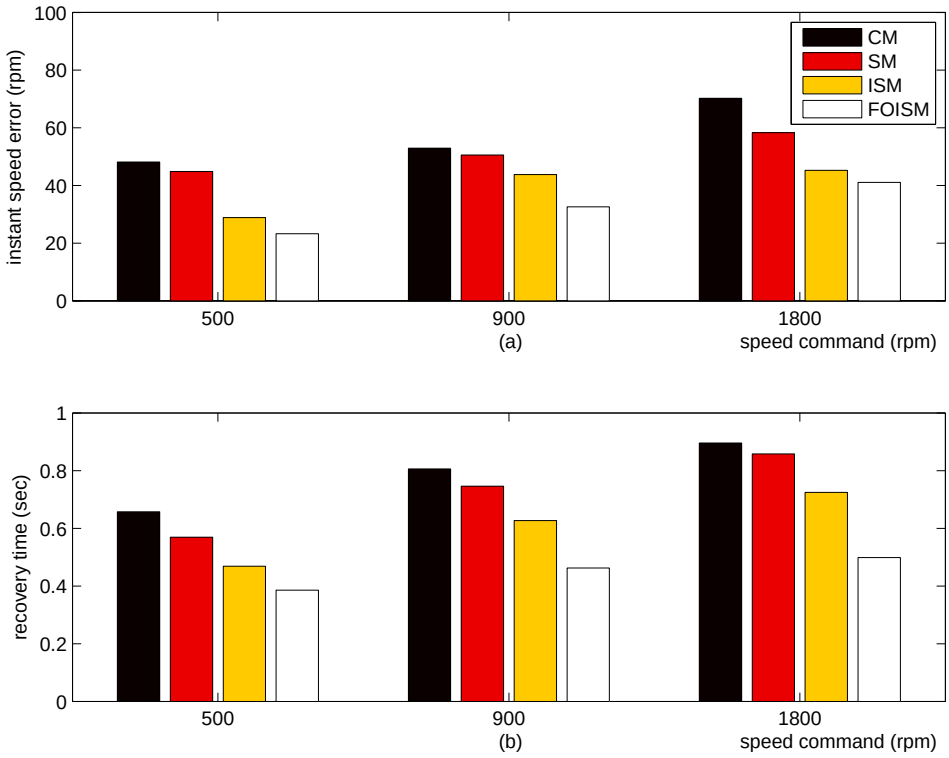

FIGURE 13. Experimental results of speed transient responses with load suddenly applied: (a) tracking error, (b) recovery time

[16] C. Ma and Y. Hori, Fractional-order control: Theory and applications in motion control, *IEEE Trans. on Industrial Electronics Magazine*, vol.1, no.4, pp.6-16, 2007.

[17] I. Podlubny, Fractional-order systems and $PI^{\lambda}D^{\mu}$-controllers, *IEEE Trans. on Automatic Control*, vol.44, no.1, pp.208-214, 1999.

[18] H. S. Li, Y. Luo and Y. Q. Chen, A fractional order proportional and derivative (FOPD) motion controller: Tuning rule and experiments, *IEEE Trans. on Control System Technology*, vol.18, no.2, pp.516-520, 2010.

[19] I. Podlubny, Geometric and physical interpretation of fractional integration and fractional differentiation, *Fractional Calculus & Applied Analysis*, vol.5, no.4, pp.367-386, 2002.

[20] M. S. Tavazoei, M. Haeri and S. Jafari, Fractional controller to stabilize fixed points of uncertain chaotic systems: Theoretical and experimental study, *Proc. of IMechE, Part I: J. Systems and Control Engineering*, vol.222, no.3, pp.175-184, 2008.

[21] H. Delavari, R. Ghaderi, A. Ranjbar and S. Momani, Fuzzy fractional order sliding mode controller for nonlinear systems, *Communications in Nonlinear Science and Numerical Simulation*, vol.15, no.4, pp.963-978, 2010.

[22] A. J. Calderón, B. M. Vinagre and V. Feliu, Fractional order control strategies for power electronic buck converters, *Signal Processing*, vol.86, no.10, pp.2803-2819, 2006.

[23] D. W. Novotny and T. A. Lipo, *Vector Control and Dynamics of AC Drives*, Oxford University Press, Great Britain, New York, 1996.

[24] I. Podlubny, *Fractional Differential Equations*, Academic Press, San Diego, CA, 1999.

[25] Y. G. Cao, Y. Li, W. Ren and Y. Q. Chen, Distributed coordination of networked fractional-order systems, *IEEE Trans. on Systems, Man, and Cybernetics – Part B: Cybernetics*, vol.40, no.2, pp.362-370, 2010.

[26] A. Oustaloup, F. Levron, B. Mathieu and F. M. Nanot, Frequency-band complex noninteger differentiator: Characterization and synthesis, *IEEE Trans. on Circuits and Systems – I: Fundamental Theory and Applications*, vol.47, no.1, pp.25-39, 2000.

[27] B. Vinagre, I. Podlubny, A. Hernandez and V. Feliu, Some approximations of fractional order operators used in control theory and applications, *Fractional Calculus & Applied Analysis*, vol.3, no.3, pp.231-248, 2000.

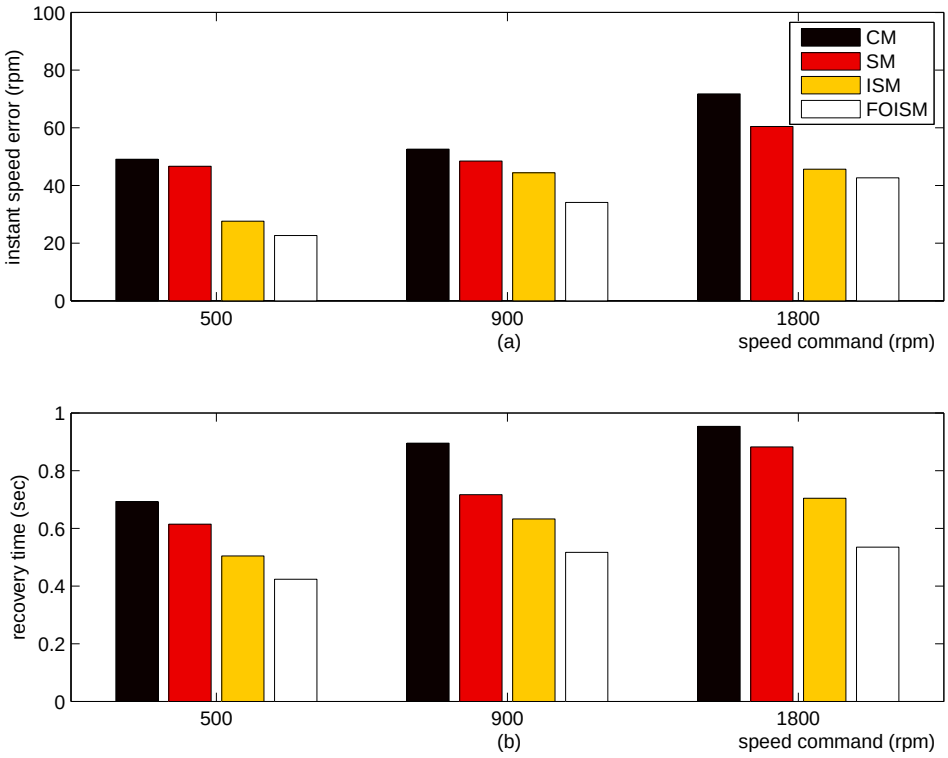

FIGURE 14. Experimental results of speed transient responses with load suddenly removed: (a) tracking error, (b) recovery time

[28] H. Rehman, A. Derdiyok, M. K. Guven and L. Xu, A new current model flux observer for wide speed range sensorless control of an induction machine, *IEEE Trans. on Power Electronics*, vol.17, no.6, pp.1041-1048, 2002.

[29] M. Demirtas, DSP-based sliding mode speed control of induction motor using neuro-genetic structure, *Expert Systems with Applications*, vol.36, no.3(I), pp.5533-5540, 2009.

[30] M. A. Duarte-Mermoud, F. J. Mira, I. S. Pelissier and J. C. Travieso-Torres, Evaluation of a fractional order PI controller applied to induction motor speed control, *The 8th IEEE International Conference on Control and Automation*, Xiamen, China, pp.573-577, 2010.

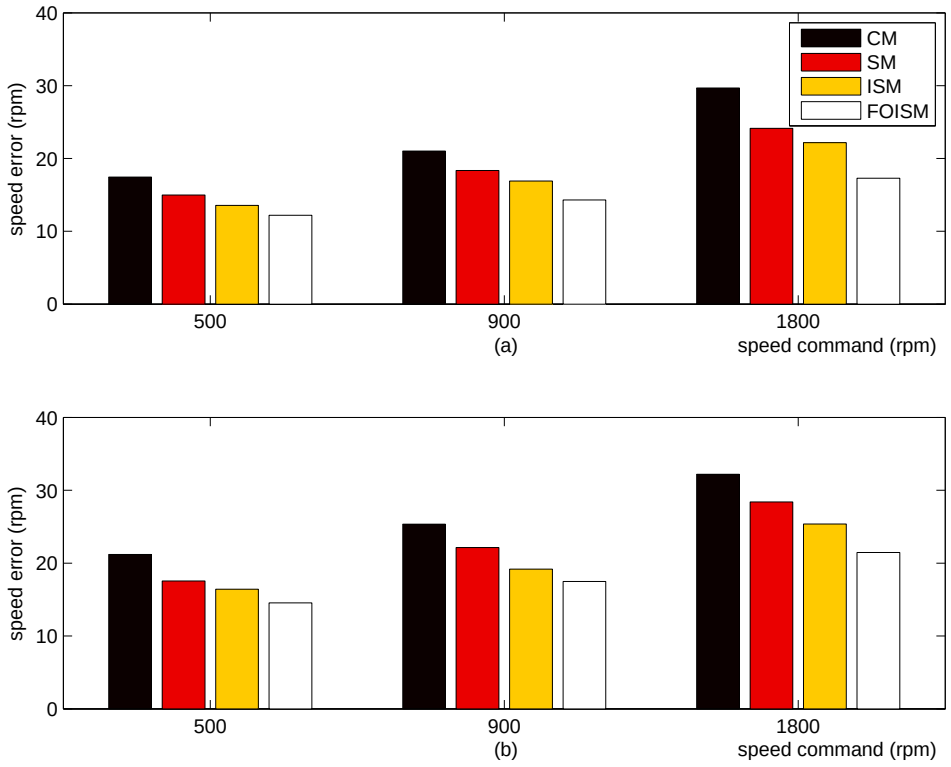

FIGURE 15. Experimental results of speed steady-state errors with different methods: (a) without load, (b) load applied

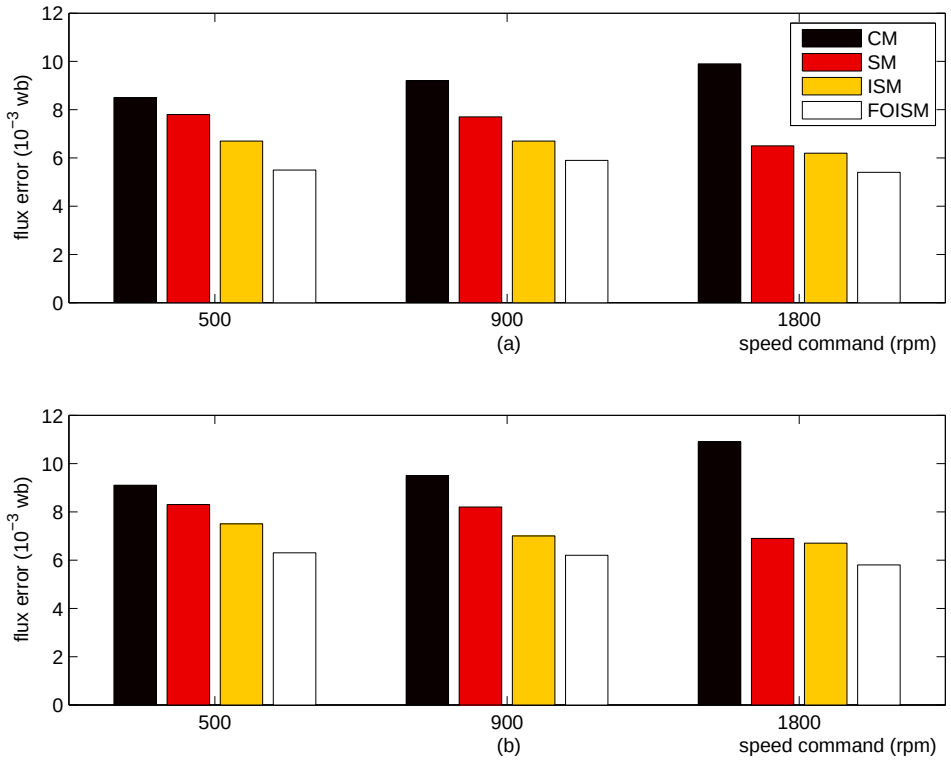

FIGURE 16. Experimental results of flux steady-state errors with different methods: (a) without load, (b) load applied